Supporting Information

Scalable 2-tier protruding micro-/nano-optoelectrode arrays with hybrid optical-electrical modalities by hierarchical modular design

Elieser Mejia, Junyeob Song, Yuming Zhao, Yizhou Qian, Chuan Xiao, Henri J. Lezec, Amit Agrawal, and Wei Zhou*

Experimental Section

Fabrication and transfer of AuNHA on hierarchical surfaces

To create AuNHA deposition masks, we used our established protocol adapted from the phase-shifting photolithography, etching, electron-beam deposition and lift-off (PEEL) technique.[1] Briefly, we used a free-standing film of AuNHA as a physical deposition mask to create periodic arrays of discrete multilayered nanoantennas. To fabricate AuNHA, we first used a poly(dimethylsiloxane) (PDMS) photomask replicated from a silicon master patterned with nanopillar arrays to expose a positive-tone photoresist (PR) on a silicon wafer in contact mode. After exposure and development of PR nanopillar arrays, we deposited a thin Cr layer (nominally 10 nm) using physical vapor deposition (PVD) by electron-beam (e-beam) evaporation, followed by sonication with acetone to lift off the nanopillar arrays and create Cr nanohole arrays on the silicon wafer. Using reactive ion etching with O_2 and CF_4 mixtures (1:5), we etched an undercut in the silicon wafer under the Cr nanohole arrays, followed by the e-beam PVD of approximately 160 nm thick Au layer on top of the Cr. We then lifted off AuNHA using Cr etchant and handled the thin film with a plasma-treated glass slide, scooping it from the Cr etchant dish and transferring it to a water-filled dish. We transferred the AuNHA onto the micropillar electrode array from the water dish by suspending and transporting the AuNHA

in a water droplet on the glass slide. After transferring AuNHA by tilting the glass slide over the center of the MEA, we allowed the water droplet underneath the AuNHA to evaporate steadily at room temperature. Note that the rapid evaporation by applied heat can result in the AuNHA film wrapping/compressing onto the pillar.

Fabrication of micro-/nano-optoelectrode arrays

The fabrication of micro-/nano-optoelectrode begins by precleaning a three-inch diameter Si wafer with oxygen plasma (50 W, 1 min, 50 cm^3/min of O_2) and followed by spin-coating with positive-tone photoresist (PR) at 3000 revolutions per min for 30 s. The resist is then prebaked on a hotplate set for 2 min at 95 °C, and the mask design #1, containing micropillar arrays, is exposed onto SU8 using a maskless aligner (direct-write photolithography, DWPL). We leveraged the automated features of the DWPL tool to quickly generate a focus-exposure matrix, allowing us to determine the optimal exposure dose around 100 mJ/cm^2 with the 375 nm laser and optimal defocus value around 0. After PR exposure, the exposed PR on the silicon wafer is baked using a hot plate for 3 min at 95 °C, and the pattern is developed by immersing the wafer in a dish containing SU8 developer for approximately 2 min to 3 min. Next, the wafer is rinsed with isopropyl alcohol and blow-dried with N_2 flow. Lastly, the target SU8 micropillar structures on the silicon wafer are hard baked at 180 ºC for 45 mins. Following a similar procedure, we prepared a bilayer resist stack by first spin-coating a lift-off resist at 3000 revolutions per min for 45 s, followed by baking on a hotplate set at 180 °C for 5 mins; the second layer consisting of positive photoresist is spin-coated at 4000 revolutions per min and baked at 115 °C for 1 min. We exposed our mask design #2, which consisted of the microelectrodes, contact pads, and lines. Similar to before, a focus-exposure matrix was used to find the optimal exposure and focus with 405 nm wavelength laser conditions around 150 mJ/cm^2 and 0, respectively. Alignment markers were patterned to ensure proper overlap between each square microelectrode and 4 x 4 micropillar array. After PR exposure, the wafer

is immersed in tetramethylammonium hydroxide (TMAH) for approximately 1 min and 40 s to create an undercut in the lift-off layer and transferred to a dish containing deionized (DI) water for 30 s to stop the development process. We rinsed any excess exposed PR with DI water, gently streamed from a wash bottle. Any excess resist beyond development can be "descummed" using plasma treatment, but we found the procedure worked successfully without descumming before deposition. We used the direct current and radio-frequency sputtering guns in a commercial sputtering PVD system to deposit 10 nm of SiO_2, 30 nm of Cr, and 100 nm of Au while the substrate rotated. Sputter PVD is followed by the spin-coating of a positive PR which was then soft-baked and exposed to define a clear window for only the 64 square microelectrode regions with the rest of the wafer being masked. The prefabricated AuNHA was then transferred onto the wafer, and e-beam PVD was conducted without substrate rotation to deposit alternating layers of 12 nm thick Au and 9 nm thick SiO_2 layers with 1 nm thick Ti interfacial adhesion layer between each metal-insulator interface. The deposition was performed at a high vacuum $< 1.33 \times 10^{-4}$ Pa. After e-beam PVD, the wafer was submerged in a double PR stripper bath for 2 h, with the development processes accelerated by periodic agitation from shaking the bath dish. After completing the lift-off process, a final passivation layer composed of SU8 can be spin-coated, prebaked, exposed, post-exposure baked, developed, and hard baked similarly as the micropillar fabrication procedure. Additionally, mesh electronics can be derived from this fabrication procedure by including a Ni sacrificial layer and a bottom passivation layer before creating the SU8 micropillars.

Micro-reflectance measurement

Reflectance measurements were done using a halogen lamp coupled to an input optical fiber connected to a confocal microscope through an adapter with a collimation lens. After passing a 50/50 beam splitter, the unpolarized light was focused at normal incidence and captured using

a 50x objective with a numerical aperture (NA) of 0.75. After passing the 50/50 beam splitter, the reflected light was collected/coupled with an output optical fiber, serving as a pinhole for spatial filtering. The output optical fiber is routed to a spectrometer. An integration time of 0.1 s was used, and an accumulation of 10 spectra was acquired for 7 single micro-/nanoelectrodes, which were then averaged to obtain the spectra shown in **Fig. 2a**. Normalization of the incident white light spectral profile and intensity was performed with a silver mirror.

FDTD simulation

As a first-order approximation, a finite 3x3 array of nanoantennas on a planar-top gold micropillar with a diameter of 2.5 μm substrate was used to simulate the response from the top of the micropillar. Optical constants of Au were taken from Johnson and Christy[2] in the spectrum range from 500 nm to 900 nm, and n = 1.5 was used for SiO_2. A fine mesh with the geometry 200 nm x 200 nm x 200 nm and mesh resolution of x = y = 3 nm and z = 1 nm was used for all nanolaminate nanoantennas. A Gaussian beam was used as the excitation source with a waist diameter of 2.6 μm, and the boundary conditions were satisfied with a phase match layer on all quadrants.

*BZT Raman measurements and SERS EF*

Samples were incubated in an ethanol-based 1 mmol/L BZT solution for 24 h, followed by ethanol rinsing to form a self-assembled monolayer on the electrode surface. SERS measurements were done under laser excitation at a wavelength of 785 nm and power of 1 mW via a 50×objective (NA = 0.75) with a commercial confocal microscope in the backscattering configuration. 2D Raman maps were acquired at a 1 s integration time per pixel over a 35 μm × 35 μm area using a piezo stage to scan the samples and a CCD camera in a commercial spectrometer to measure the Stokes Raman scattering. A long-pass filter was used to block

elastically scattered light at the wavelength corresponding to the laser line (Rayleigh scattering), and the Stokes scattering passed through a multimode fiber (100 μm core diameter) with the cleaved fiber core acting as the confocal pinhole. The SERS EFs were calculated based on our past work using the following relation, $EF = (I_{SERS}/I_{Raman}) \times (N_{Raman}/N_{SERS})$. I_{SERS}, I_{Raman}, N_{SERS}, and N_{Raman} are the SERS BZT intensity, neat BZT Raman intensity, and the number of BZT molecules contributing to SERS and neat Raman intensities, respectively. I_{SERS} (1073 cm^{-1}), which corresponds to the C-C-C ring in-plane breathing mode, was used for the EF calculations. N_{SERS} was calculated by $N_{SERS} = SA \times \rho_{SERS}$, where SA is the metal surface area contributing to the enhancement of Raman signal and ρ_{SERS} is the packing density of BZT on Au surface; The packing density of BZT molecules is 6.8×10^{14}/cm^2. N_{Raman} was calculated by $N_{Raman} = A \times d_{eff} \times \rho_{BZT}$, where A is the focused illumination area, d_{eff} is an effective depth; The number density of neat BZT, ρ_{BZT}, is 5.9×10^{21}/cm^3.


Electrochemical measurement

Potentiostatic electrochemical impedance spectroscopy (EIS) was conducted with the working electrode voltage (E_{we}) set to zero vs. open circuit and a sinus amplitude of 10 mV. The equivalent circuit model assumes a current-less situation (I_{dc}=0) with no applied direct current or voltage. An Ag/AgCl saturated in KCl was used as the reference electrode, and a platinum coil was used as the counter electrode in a custom electrochemical cell (EC-cell) mounted to the sample using adhesive stripes. Phosphate buffer saline (PBS) was used as the electrolyte solution, composed of NaCl: 0.137 mol/L, KCl: 0.0027 mol/L, Na_2HPO_4: 0.01 mol/L, KH_2PO_4: 0.0018 mol/L for standard 1x PBS from commercial suppliers. Approximately 2 mL of 1x PBS was dropped into EC-cell, and measurements were done at room temperature. A potentiostat was used to perform EIS and cyclic voltammetry (CV), ranging from –0.5 V to 0.5 V in 100

mV/s increments. CV measurements were cycled several times until the EC system reached a steady state with the same CV profile shown in **Fig. 4**.
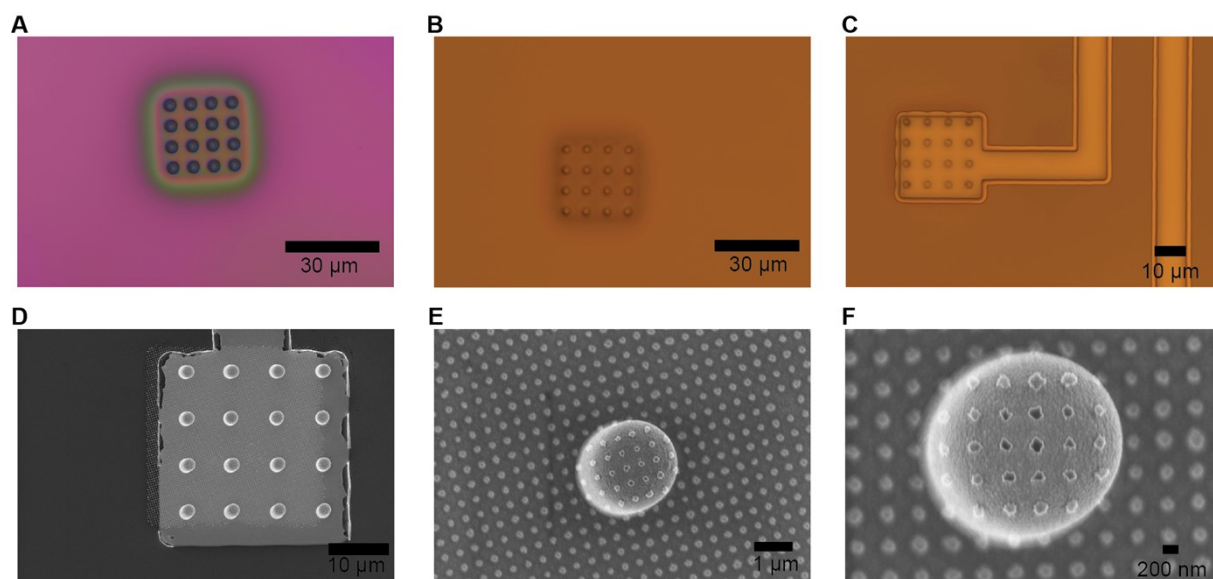
Fig. S1. Intermediate fabrication steps and final structure imaged with optical microscope and SEM. Optical images show (A) Lift-off resist (LOR) around pillar array, (B) PR-LOR bilayer resist stack, (C) development of PR and undercut of LOR revealing electrodes and contact lines. SEM images show (D) electrode with protruding out-of-plane micropillars and nanoantenna array, (E) single micropillar with nanoantenna array at the base, (F) shape variation of nanoantennas on top of the micropillar.
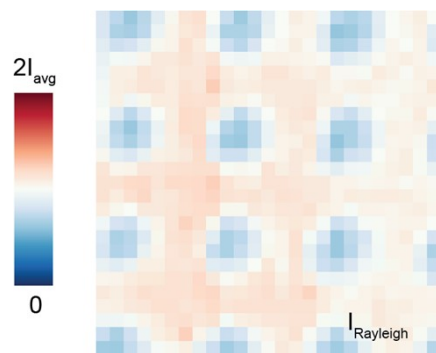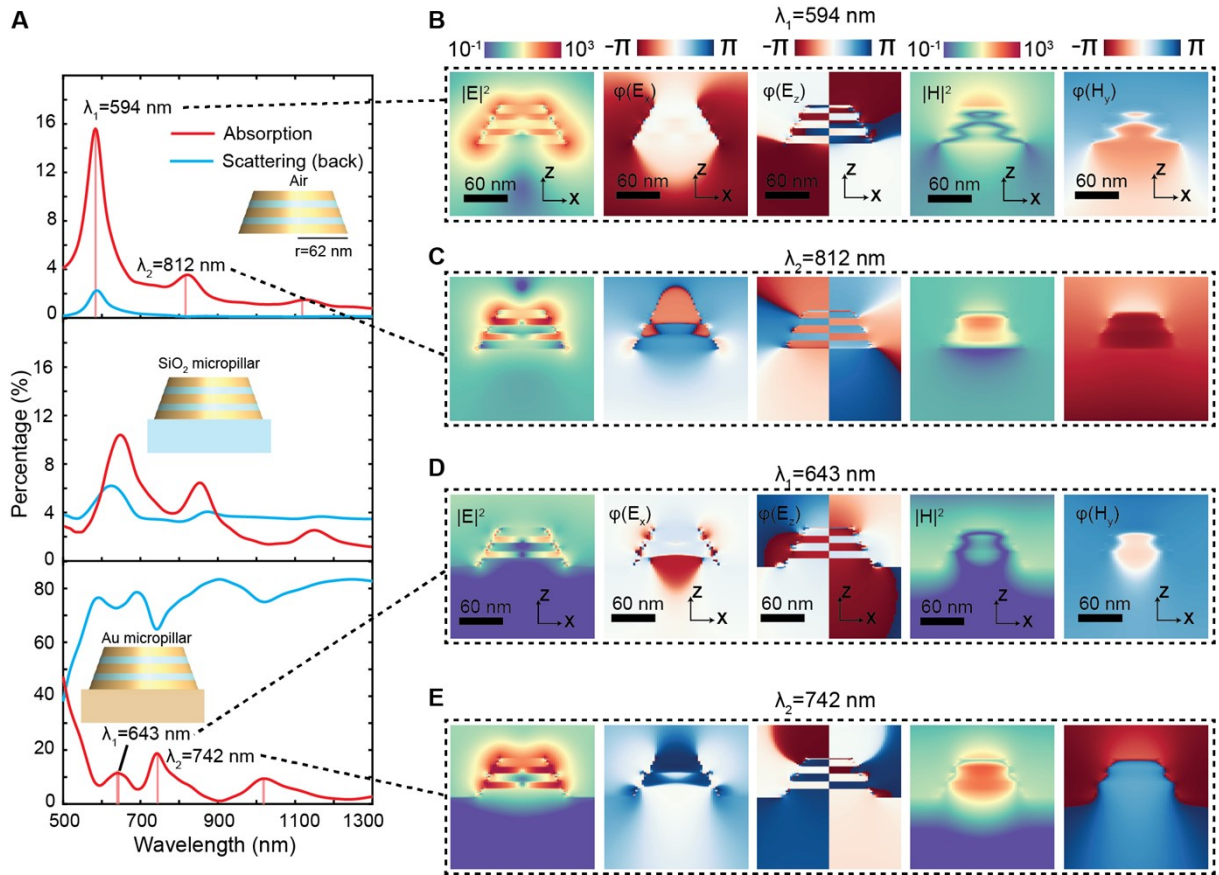
**Fig. S2**. Confocal Raman image of Rayleigh scattering peak (0 cm^{-1}).
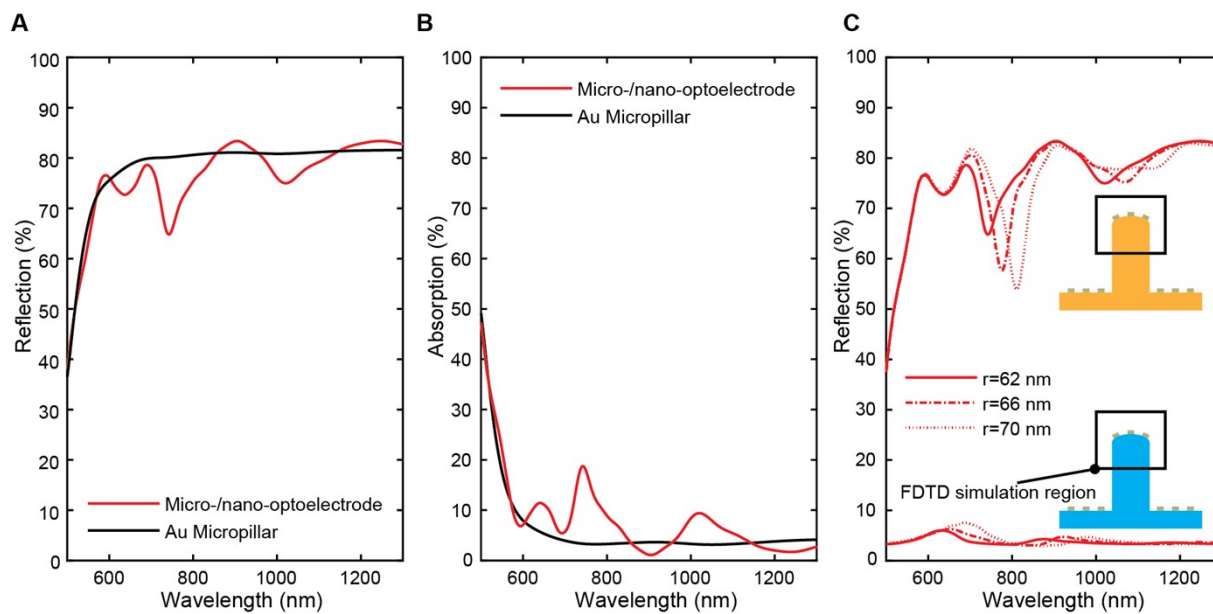
Fig. S3. FDTD-calculated optical response. (A) Reflection and (B) absorption spectra for both micro-/nano-optoelectrode and Au micropillar. (C) Reflection spectra for dielectric and conductive micro-/nano-optoelectrode with nanoantennas of increasing diameter from 124 nm to 140 nm.

Fig. S4. FDTD-calculated far- and near-field response of nanoantenna in air and on a SiO_2 and Au micropillar (ground plane). (A) Absorption and backscattering for nanoantenna in air and on a SiO_2 micropillar and Au ground plane. (B-E) FDTD calculated near-field distribution maps of $|E|^2$, $\varphi(E_z)$, $\varphi(E_x)$, $|H|^2$, and $\varphi(H_y)$ at the *x-z* plane for resonant modes at (B) $\lambda_1 = 594$ nm and (C) $\lambda_2 = 812$ nm for nanoantenna in air and (D) $\lambda_1 = 643$ nm and (E) $\lambda_2 = 742$ nm on ground plane.

9
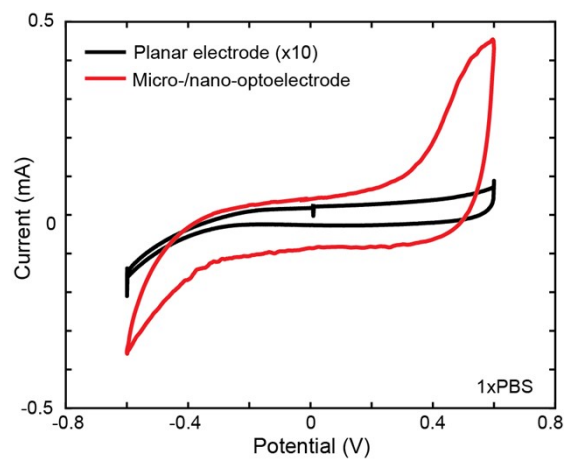
Fig. S5. Cyclic voltammogram with linear current scale for planar electrode and micro-/nano-optoelectrode.

References

1. J. Henzie, M. H. Lee and T. W. Odom, *Nat Nanotechnol*, 2007, **2**, 549-554.

2. P. B. Johnson and R. W. Christy, *Physical Review B*, 1972, **6**, 4370-4379.